Recapitulation of growth factor-enriched microenvironment via BMP receptor activating hydrogel

Qinghao Zhang [a,b,c,d,**], Yuanda Liu [a,b,c,d], Jie Li [a,b,c,d], Jing Wang [a,b,c,e,*], Changsheng Liu [a,b,c,d,***]

[a] Material Science and Engineering School, East China University of Science and Technology, Shanghai, 200237, PR China
[b] Engineering Research Center for Biomedical Materials of Ministry of Education, East China University of Science and Technology, Shanghai, 200237, PR China
[c] Key Laboratory for Ultrafine Materials of Ministry of Education, East China University of Science and Technology, Shanghai, 200237, PR China
[d] Frontiers Science Center for Materiobiology and Dynamic Chemistry, East China University of Science and Technology, Meilong Road 130, Shanghai, 200237, PR China
[e] The State Key Laboratory of Bioreactor Engineering, East China University of Science and Technology, Shanghai, 200237, PR China

ARTICLE INFO

ABSTRACT

Exposure to a growth factor abundant milieu has remarkable regenerative and rejuvenating effects on organ diseases, tissue damage, and regeneration, including skeletal system defects and bone regeneration. Although the introduction of candidate growth factors into relevant fields has been reported, their regenerative effects remain unsatisfactory, mainly because of the experimental challenges with limited types of growth factors, elusive dosage adjustment, and asynchronous stem cell activation with cytokine secretion. Here, an innovative hydrogel recapitulating a growth factor-enriched microenvironment (GEM) for regenerative advantage, is reported. This sulfated hydrogel includes bone morphogenetic protein-2 (BMP-2), an essential growth factor in osteogenesis, to direct mesenchymal stem cell (MSC) differentiation, stimulate cell proliferation, and improve bone formation. The semi-synthetic hydrogel, sulfonated gelatin (S-Gelatin), can amplify BMP-2 signaling in mouse MSCs by enhancing the binding between BMP-2 and BMP-2 type II receptors (BMPR2), which are located on MSC nuclei and activated by the hydrogel. Importantly, the dramatically improved cytokine secretion of MSCs throughout regeneration confirms the growth factor-acquiring potential of S-Gelatin/rhBMP-2 hydrogel, leading to the vascularization enhancement. These findings provide a new strategy to achieve an *in situ* GEM and accelerated bone regeneration by amplifying the regenerative capacity of rhBMP-2 and capturing endogenous growth factors.

1. Introduction

Currently, studies on the human skeleton system have revealed that its notable capability of bone remodeling and regeneration following injuries and diseases are mainly due to the presence of resident stem cells, especially mesenchymal stem cells (MSCs) [1,2]. MSCs have an essential role in maintaining bone remodeling and dominating bone repair. They can remain dormant in a quiescent condition and can be stimulated by damage or stress signals, such as mechanical stimuli, electrical signals, and growth factors [3–5]. The quiescent MSCs undergo division for self-renewal, secrete growth factors for proliferation and differentiation, and induce osteogenesis to complete the bone regeneration process [6,7]. Evidently, this regeneration process is influenced by a dynamic interplay between intrinsic factors within MSCs and cellular/acellular extrinsic factors including angiogenesis and growth factors [8,9]. However, as reported by a growing number of studies, the regenerative capacity of MSCs diminish under abnormal conditions, such as diabetes and aging, which leads to a slow and incomplete recovery process after injury [10–12]. Although quiescent MSCs continue to be present in the niche, their self-renewal capacity is compromised due to the triggered responses such as cell inactivation or growth factor deficiency, thus resulting in a reduction in the function and quantity of the osteogenic stem cell pool. These events contribute to the delay in bone repair and may cause incurable bone defects.

Consequently, there is an urgent need for novel tissue engineering strategies to treat bone defects, especially as deficits in bone function and disruption of the normal ecological niche may directly correlate to morbidity and mortality.

As important components of the extracellular matrix (ECM) and essential dominators of cellular activities, growth factors have been highlighted in bioengineering, biomaterials science, and other related fields. In orthopedic medicine, two BMP family growth factors, BMP2 and BMP7, are approved by the United States Food and Drug Administration (FDA) for use clinical therapy because of their crucial effects on the sequential cellular activities for bone regeneration, indicating their potent ability to induce osteogenesis and bone formation [13]. However, the serious side effects of high drug doses, including FDA-approved BMP-2, have limited their usage [14,15]. Further, the short half-life of BMP-2 in the bloodstream and its burst release resulting from physical adsorption in scaffolds have prompted the development of more efficient biomaterials and drug delivery techniques for BMP-2-based therapies with dose reduction to resolve adverse responses and to promote strong endogenous bone regeneration.

Recent studies have demonstrated that growth factor recruitment to the *in situ* locations can improve damaged tissues under abnormal conditions. Intriguingly, the introduction of growth factors restores the regenerative capacity of endogenous MSCs in the microenvironment [16–19], thus accelerating tissue formation [20,21]. The continuous access is thought to boost multiple stem cell functions and attenuate vascularization by releasing growth factors into circulation. Moreover, recent studies [22–24] revealed potential systemic factors that are responsible for regeneration, demonstrating the importance of endogenous growth factors in tissue repair. Despite such importance in tissue repair and tremendous therapeutic promise in clinic, the biochemical and cellular mechanisms by which growth factors regulate regeneration remain underexplored, which restricts the consideration of growth factors for treatment of bone defects. Such condition also influenced in the field of biomaterials. A few studies reported biomaterials with direct regulation to growth factors or growth factor receptors, such as sulfated chitosan [25], sulfated polysaccharides [26], miRNAs [27], and integrins [28]. Among them, the effect of sulfonation group has been concentrated, while the understanding for their regulation mechanisms

to growth factors is still unrevealed. Ulteriorly, this gap, partially resulting from the complexity of the *in vivo* microenvironment and the dynamic nature of growth factors, greatly blocks up the construction of integral GEM artificially with exogenous growth factors. Thus, designing a biomaterial to capture endogenous growth factors and recapitulate a GEM has been a promising strategy for cell niche mimicking.

Therefore, this study presented a hydrogel for the establishment of *in situ* GEM via endogenous growth factors. We examined the role of the sulfated group from collagen derivatives in promoting the osteoinductive capacity of BMP-2 via BMP-BMPR interaction. With the amplifying of BMP-2 signals, including MSCs differentiation regulation and cytokine secretion improvement, the osteogenesis and vascularization was enhanced, resulting from BMPR2/Smad pathway activation and the enrichment of growth factors and stem cells. *In vitro* cell-based osteogenic assays were used to evaluate the biological activity of BMP-2 combined with two collagen derivatives (gelatin and S-Gelatin), such as cell viability, alkaline phosphatase (ALP) activity, and matrix mineralization. The binding availability of BMP-2 and BMPRs influenced by sulfonated derivatives was examined using immunostaining. Furthermore, RNA quantification and western blotting for protein expression verified the BMPR2/Smad/OPN pathway activation. The recruitment of mesenchymal stem cells (MSCs) and multiple growth factors was also examined in the scaffolds after initial implantation (Scheme 1). Finally, an ectopic bone implantation model was implemented to verify the potency of S-Gelatin on BMP-2-induced osteogenesis and vascularization *in vivo*.

2. Experimental section

Preparation of Gelatin/rhBMP-2 hydrogel and S-Gelatin/rhBMP-2 hydrogel: Gelatin/rhBMP-2 hydrogels and S-Gelatin/rhBMP-2 hydrogels were prepared by loading rhBMP-2 (donated by Shanghai Rebone biological materials co., LTD, China) into the gelatin hydrogel and sulfonated gelatin hydrogel. (Fig. 1A). Prior to preparing the sulfonated gelatin hydrogel, a sulfonated gelatin prepolymer was first synthesized through grafting a sulfonic acid group onto gelatin backbone according to Fig. S1. 2.2 g of gelatin(Sigma-Aldrich,V900863-500G) was added to 20 mL hydrochloric acid (PH = 2) and dissolved the gelatin at 60 °C.

Improve Bone Regeneration

BMPR2 Activation and Osteogenesis

Angiogensis and Osteogenesis

Scheme 1. Illustration for hydrogel-induced secretion of growth factors and recruitment cells to recapitulate *in situ* osteogenesis for bone regeneration. S-Gelatin/rhBMP-2 hydrogels were prepared for bone regeneration, wherein S-Gelatin hydrogel was used as a matrix for rhBMP-2 loading by lyophilization. After implantation, the S-Gelatin/rhBMP-2 hydrogels could rapidly activate BMPR2 on MSCs to induce differentiation and cytokine secretion. In the process the BMPR2/Smad/OPN pathway was stimulated and resulted into osteogenesis enhancement. During tissue formation, the S-Gelatin/rhBMP-2 could additionally regulate the secretion of endogenous growth factors, mimicking a stem cell microenvironment with growth factor enrichment to accelerate bone tissue regeneration.
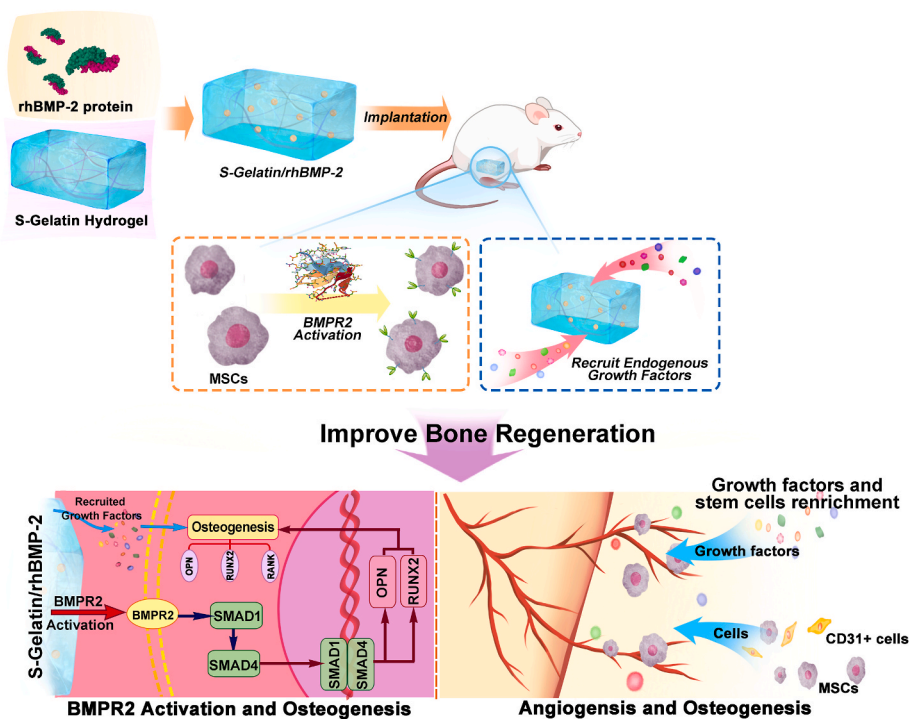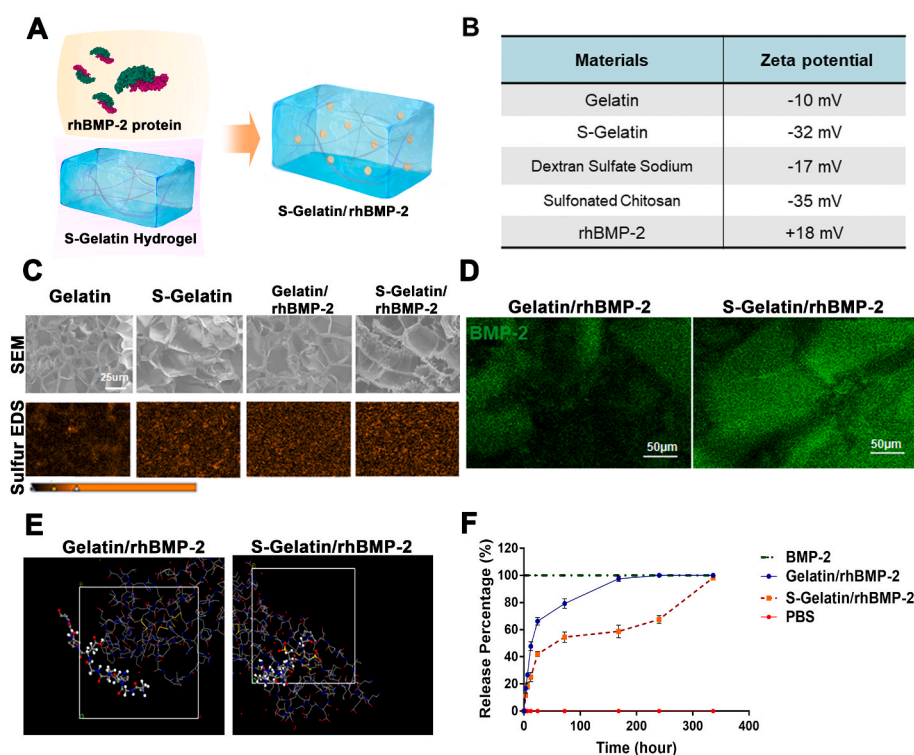
Fig. 1. Material characterization for the S-Gelatin/rhBMP-2 hydrogel. A) Schematic of the S-Gelatin/rhBMP-2 hydrogel fabrication process. B) Electronegativity of S-Gelatin hydrogels. With the sulfonated groups, S-Gelatin showed stronger electronegativity. C) Scanning electron micrographs and sulfur-based energy dispersive X-Ray spectroscopy of Gelatin, S-Gelatin, Gelatin/rhBMP-2, and S-Gelatin/rhBMP-2. D) Immunofluorescence staining for BMP-2 distribution in Gelatin/rhBMP-2, and S-Gelatin/rhBMP-2. E) Monte Carlo Simulation for the BMP-2/gelatin and BMP-2/sulfonated gelatin mixed systems in aqueous conditions. The ball-and-stick model represents the structure of S-Gelatin, and the line model represents the structure of rhBMP-2 downloaded from the Protein Data Bank F) BMP-2 release from Gelatin/rhBMP-2, and S-Gelatin/rhBMP-2 into phosphate buffered saline solution. The release representing time is continuous up to 336 h.

With stirring, 600 μL glycidyl methacrylate(GMA)(Shanghai Aladdin Bio-Chem Technology Co, LTD, China) was drop-wised to the above gelatin solution. After reacting for 6 h, 600 μL H_2O_2 was added to the above solution. After reacting for 6 h, 1 mL 30%(w/v) $NaHSO_3$ was drop-wised to the solution at 0.5 mL per minute and reacted at 50 °C for 2 h. After the sulfonating reaction, the following solution was dialyzed against ultrapure water at 37 °C for 24 h with a 2000Da Mw cut-off dialysis membrane. The dialysis product was poured to 20 mL ethyl alcohol and centrifuged three times at 8000 rpm for 15min to retain the supernatant. Adjusted the solution's PH to 7.35, and lyophilized for 3 d to get purified sulfonated gelatin.Next, gelatin hydrogel and sulfonated gelatin hydrogel were prepared by mixing 0.5%(w/v) genipin (Dibai, Shanghai, China) and 6%(w/v) gelatin solution or sulfonated gelatin solution to crosslink at 60 °C. Finally, Gelatin/rhBMP-2 hydrogel and S-Gelatin/rhBMP-2 hydrogel were formed by dropping 30 μg rhBMP-2 onto gelatin hydrogel and S-Gelatin hydrogel and stayed a while to be totally absorbed.

S-Gelatin/rhBMP-2 hydrogels characterization: First, scanning electron microscopy (S-4800, Hitachi, Tokyo, Japan) were used to observe the pore size of the Gelatin/rhBMP-2 hydrogel and S-Gelatin/rhBMP-2 hydrogel after being sputter-coated with gold. During the scanning, EDS was used to detect the sulfur on the surface of the S-Gelatin/rhBMP-2. Next, immunofluorescence staining for BMP-2 was used to verify the rhBMP-2 loaded on the gelatin hydrogel and S-Gelatin hydrogel. The hydrogels were fixed with 4% paraformaldehyde for 1day at 4 °C. After being dehydrated through a graded ethanol series and cleared into 4.5 mm slices with a slicer(Leica 4 SP1600 Saw Microtome system, Germany) and stained with anti-BMP-2 antibody at 4 °C overnight. Sections were stained with the appropriate secondary antibody, and sections were imaged using a laser confocal microscope(Nikon A1R). In addition, Materials Studio software was used to the simulate the conformation between the S-Gelatin and rhBMP-2. Finally, the release of rhBMP-2 on the gelatin/rhBMP-2 hydrogel and S-Gelatin/rhBMP-2 hydrogel was detected by a Human BMP-2 ELISA kit (Neobioscience, Shenzhen).The hydrogels were immersed in 2 mL of 0.01 M PBS solution and incubated in a 37 °C shaker incubator. And the supernatants at 4 h, 8 h, 12 h, 1 d, 3

d, 7 d, 14 d were collected and the concentration of rhBMP-2 in the supernatant was testing by the Elisa kit according to the product description.

Cell isolation and culture: For mouse bone marrow mesenchymal stem cells (mBMSCs) isolation and expansion, after 8-week-old male C57BL/6 mice were euthanasized. The isolated bone marrow cells were allowed to recover and adhere in Dulbecco's minimum essential medium (DMEM) with 10% fetal bovine serum(FBS) and 1% penicillin/streptomycin for 18 h, Thereafter, the nonadherent cells were removed by rinsing several times with PBS and fresh growth medium was added. mBMSCs were maintained at 37 °C in 100% humidified air containing 5% carbon dioxide, with the medium changed every other day.

Circular dichroism (CD) analysis: In this study, Circular dichroism was used to analyze the conformation changes of rhBMP-2 before and after interaction with gelatin and sulfonated gelatin. The gelatin and sulfonated gelatin solution were prepared and mixed with rhBMP-2 solution. The circular dichroism changes were detected and compared with the rhBMP-2 solution with the detection wavelength ranged from 190 to 260 nm. Specific changes in the conformation of the rhBMP-2 were calculated using CDNN software.

MTT assay in vitro: According to GB/T 16776.5–2017/ISO10993–5:2009 a clause in the State Standard of the People's Republic of China for biologic evaluation of medical devices-Part 5 test for *in vitro* cytotoxicity, the hydrogels of were added into 48-well plates, and mBMSCs were seeded on the surface of the materials to construct a 3D culture (above 1.0×10^4 cells per well, with each sample having five parallel controls).After 1- or 3-days' co-culturing, the cell proliferation was evaluated by MTT assay. Added MTT (Aladdin Bio-Chem Technology Co., Ltd, China) solution into each well, which were then incubated in a swing bed at 37 °C for 4 h. And then, the supernatant was removed, and the sediment was dissolved by DMSO. The optical density of each well was measured at 495 nm on a microplate reader.

ALP activity of mBMSCs in vitro: Cultured cells without (for the Control condition) or with (rhBMP-2, Gelatin hydrogels and sulfonated gelatin hydrogels with different degrees of sulfonation, Gelatin/rhBMP-2 hydrogels and S-Gelatin/rhBMP-2 hydrogels) were added into 48-well

plates. mBMSCs were seeded on the surface of the hydrogels to incubate for 7 days. The medium was refreshed every three days. To lyse the cells, 1% NP-40 solution (Beyotime, China) was added into the each well with 800 μL and cultured for 90 min at 37 °C. The lysis was collected and stored for analysis of ALP activity and total protein content. The intracellular total protein content was determined by using the micro-BCA protein assay kit (Beyotime, China) with absorbance measured at 562 nm by a Thermo Scientific Spectra Max M2 Spectrophotometer (Thermo Scientific, USA), which was used as the standard in the ALP activity normalization. ALP activity was determined by the release of p-nitrophenol from p-nitrophenyl phosphate substrate. Each reaction was activated by the addition of p-nitrophenyl phosphate to the sample solution and stopped after 3.5 h. The optical density was measured at 405 nm using the same spectrophotometer. ALP staining was performed using a BCIP/NBT ALP kit (Beyotime). Briefly, the mBMSCs were plated on the films in 48-well plates and cultured for 7 days. After fixation with 2.5% glutaraldehyde, the cells were incubated in a mixture of nitro-blue tetrazolium and 5-bromo-4-chloro-3-indolylphosphate.

Mineralization assay: mBMSCs were seeded in 24-well plates at a density of 1.0×10^4 cells/well in α-MEM (10% FBS) and incubated overnight. Subsequently, the medium was replaced with mineralization culture medium (α-MEM, 2% FBS, 10 mM ascorbic acid, and 10 mMβ-glycerol phosphate) in the presence of rhBMP-2 and scaffolds. Medium was replaced every two days. After 14 days of incubation, the cell layer was washed twice with PBS, fixed with 4% paraformaldehyde for 15 min, gently washed twice with PBS, and stained with 1% Alizarin Red S (pH = 4.2) until the mineralized ma-trix appeared red. After being washed three times with PBS, the cell layer was imaged using an inverted microscope (DMi8, Leica, Germany). Finally, quantitative analysis of mineralization was performed using 10% cetylpyridinium chloride to dissolve mineralized nodules for 30min and optical density (OD) of the samples was measured at 562 nm using a microplate reader.

Quantification of growth factors and cytokines in vitro: After 1,3,7 days of incubation with differentiation medium, conditioned medium and mBMSCs on hydrogels were collected for ELISA analysis. Briefly, the extracts of total protein were acquired by lysing cells on hydrogels in cold radioimmunoprecipitation assay (RIPA) buffer (Beyotime, China). The concentration of SDF-1α, FGF-2, Ang-1, VEGF,OPN, OPG, and RANK was measured by ELISA Kit according to the manufacturer's instructions.

Animal Surgery and mouse muscle bag implantation: Male C57BL/6 mice (6 weeks old, Slac Laboratory) were anesthetized with 2% isoflurane at a low rate of 0.4 L/min. Following hair removal and skin incision, the materials were implanted into the muscle bag at both left and right muscle bags. After 1 day 3 days 7days, 21days, and 28 days, the implants were taken out from each group of mice for subsequent experiments.

*Quantification of growth factors and cytokines in vivo:*After 1,3,7,14,28 days after implantation, the implants were removed at each time point. Subsequently, the implants were ground under liquid nitrogen and the supernatant was collected for Elisa assay.

Flow cytometry: In this study, flow cytometry was used to access cell recruitment *in vivo*. The implants were removed at each time point. Subsequently, the cells in the implants were collected by grinding the implants and filtrating with 70 μm filter. Then, the single-cell suspension was incubated with antibodies mixture for anti-mouse CD140α-APC, CD31-BV421, Ter119-PE, CD45-PE, Sca-1-PE-Cy7, CD309(VEGFR2)-Per-CP/Cy5.5. (BioLegend, USA). After 20 min, the staining was stopped by adding 1 mL cell staining buffer and the cells were washed with cell staining buffer, 300 μL of the suspension was added into the testing tubes. Finally, the samples were measured by flow cytometric analysis using a Beckman Coulter Epics XL cytometer (Beckman Coulter, USA). The gates of MSCs and αEPCs were presented in Figs. S9 and S10.

qRT-PCR: To investigate gene expression in the implants, the implants were removed at each time point. Total RNAs were extracted with Trizol reagent, followed by a reverse transcription step with PrimeScript RT reagent kit according to the manufacturer's instructions. The qRT-PCR was performed on a CFX96 Touch PCR detection system (Bio-Rad, USA) with a hot start denaturation step at 95 °C for 30 s, and then fluorescence intensity was recorded during 40 cycles at 95 °C for 5 s and 60 °C for 30 s. Murine glyceraldehyde-3-phosphate dehydrogenase (GAPDH) was used as a housekeeping gene to normalize the expression of the gene depending on the experiment.

Histochemical and immunofluenscence staining: Freshly implants were fixed overnight in 4% paraformaldehyde followed by 3 days of decalcification in 0.5 M ethylenediamineteraacetic acid (EDTA). Paraffin sections were stained with Safranin-O using standard protocols.

For immunoflurescence staining, sections were rised three times with PBST and blocked with 10% goat serum at RT for 1 h. After blocking, sections were stianed overnight at 4 with primary abtibody(anti-CD44; anti-CD90; anti-BMPR2). Sections were stained with the approprite secondary antibody, and were mounted using a prolong gold antifade reagent with DAPI. The mounted sections were imaged using a light microscope(Lcica Dmi8) or laser confocal microscope(Nikon A1R).

Western blot: To investigate the effect key proteins in TGF-β/Smad signaling pathway *in vivo*, fresh implants retrieved from ischemic mice were immediately lysed using cold RIPA buffer containing PMSF. The cell lysates were equilibrated with loading buffer to an equal concentration and boiled for 10 min. Subsequently, samples were separated by 10% SDS-PAGE at an equal concentration and then blotted on a polyvinylidene fluoride membrane. The membranes were incubated with specific antibodies to BMPR2, Smad 1/5/8 Smad 4, Runx2 and OPN followed by incubation with HRP-conjugated secondary antibody. GAPDH was used as a loading control. Visualization of the protein bands was performed with a chemiluminescence imaging system (Tanon, Shanghai, China). Total intensity of each band was determined with Tanon Image software (version 1.10; Tanon, Shanghai, China).

Transcriptome Sequencing (mRNA-seq) and Analysis: Gelatin/rhBMP-2 and S-Gelatin/rhBMP-2 samples were snap frozen in liquid nitrogen and stored at −80 °C until processing after 14 d. Then total RNA samples (three in each group) were extracted from the tissues using Trizol (Invitrogen, Carlsbad, CA, USA) according to manual instruction and analyzed by BGI seq 500 platform (BGI-Shenzhen, China). Next, oligo (dT)- attached magnetic beads were used to purify the mRNA. Then cDNA was synthesized using the mRNA fragmentation as templates. After the synthesis and purification of double stranded cDNA, the DNA termini were repaired and connected to each other. Next, fragments were amplified through polymerase chain reaction (PCR). Data quality control was performed by using Agilent 2100 Bioanalyzer and an ABI Step One Plus Real-Time PCR System. Then the library was sequenced using an Illumina HiSeq 4000. All sequencing reads were entered into the National Center for Biotechnology Information (NCBI). The Dr. Tom software was used to screen out the different genes. Finally, the KEGG pathway and Go analysis were performed by using the BLASTX algorithm.

3. Results

3.1. Material characterization

First, to verify the role of the sulfonated group in amino-acid derivatives, a sulfonated gelatin/rhBMP-2 hydrogel was synthesized as shown in Fig. S1 and Fig. 1A. GPC was used to calculate the molecular weight of Gelatin and S-Gelatin prepolymer, and the result was shown in Fig. S3. In addition, XPS was used to analyze the chemical structure of S-Gelatin prepolymer. As shown in Fig. S2(A), the absorption peak at 168eV was the electron binding energy of the 2p orbital of sulfur, which proved the successful introduction of sulfonic acid groups into gelatin backbone. Furthermore, quantitative analysis of sulfur element was used to study the effect of NaHSO₃ on the degree of sulfonation, and the results was shown in Fig. S2(B). As rhBMP-2 has a positive charge and tends to bind negatively charged materials, the zeta potential was

analyzed to evaluate the electrical properties of the materials. As shown in Fig. 2B, the S-Gelatin hydrogel possessed a higher negative charge than that of the gelatin hydrogel, indicating a stronger binding capability with rhBMP-2. Thus, after rhBMP-2 loading, the hydrogel microstructure and element scan was determined using scanning electron microscopy and energy dispersive X-ray spectroscopy, respectively. As shown in Fig. 1C, rhBMP-2 was loaded into the hydrogel-lyophilized scaffolds with favorable porosity. With the addition of sulfur from the disulfide bonds in rhBMP-2, the content of sulfur elements in S-Gelatin/rhBMP-2 scaffolds increased as indicated by the difference in S-Gelatin and Gelatin/rhBMP-2. Further, immunofluorescence staining with BMP-2 antibody, was performed to verify the function of rhBMP-2 in S-gelatin/rhBMP-2. As shown in Fig. 1D, the rhBMP-2 in the S-gelatin/rhBMP-2 hydrogel was more uniformly distributed than in the gelatin/rhBMP-2 hydrogel. As the addition of negatively charged materials is considered to stabilize rhBMP-2 aggregates, a molecular stimulation study was performed to model the combination and binding between S-Gelatin and rhBMP-2. As shown in Fig. 1E, after combination with sulfonated gelatin, rhBMP-2 demonstrated an extended conformation in

the aqueous condition instead of its collapsed compaction observed in gelatin solution, indicating that rhBMP-2 in the S-Gelatin/rhBMP-2 hydrogel was more stable compared to that in the gelatin/rhBMP-2 hydrogel. Furthermore, particle size and zeta potential were used to analyze the change of aggregation state of rhBMP-2 after the hydrogel was combined with rhBMP-2. It can be seen from Fig. S8 that the rhBMP-2 molecule in solution is positively charged and the average particle size is about 225 nm, which explained that rhBMP-2 existed in the form of aggregates in solution. After adding materials, the solution suddenly dropped to a negative charge. The average particle size of rhBMP-2 aggregates dropped to 120–190 nm; the maximum average particle size became 250 nm when the concentration of the material was 0.2 mg mL^{-1}.

Finally, the release behavior of rhBMP-2 in the hydrogels was measured using enzyme-linked immunosorbent assay (ELISA) at different time points. As shown in Fig. 1F, rhBMP-2 release from the S-Gelatin/rhBMP-2 hydrogel was slower and stably maintained compared with that from the gelatin/rhBMP-2 hydrogel, indicating that sulfonated gelatin facilitated sustained release of rhBMP-2 because of the negative
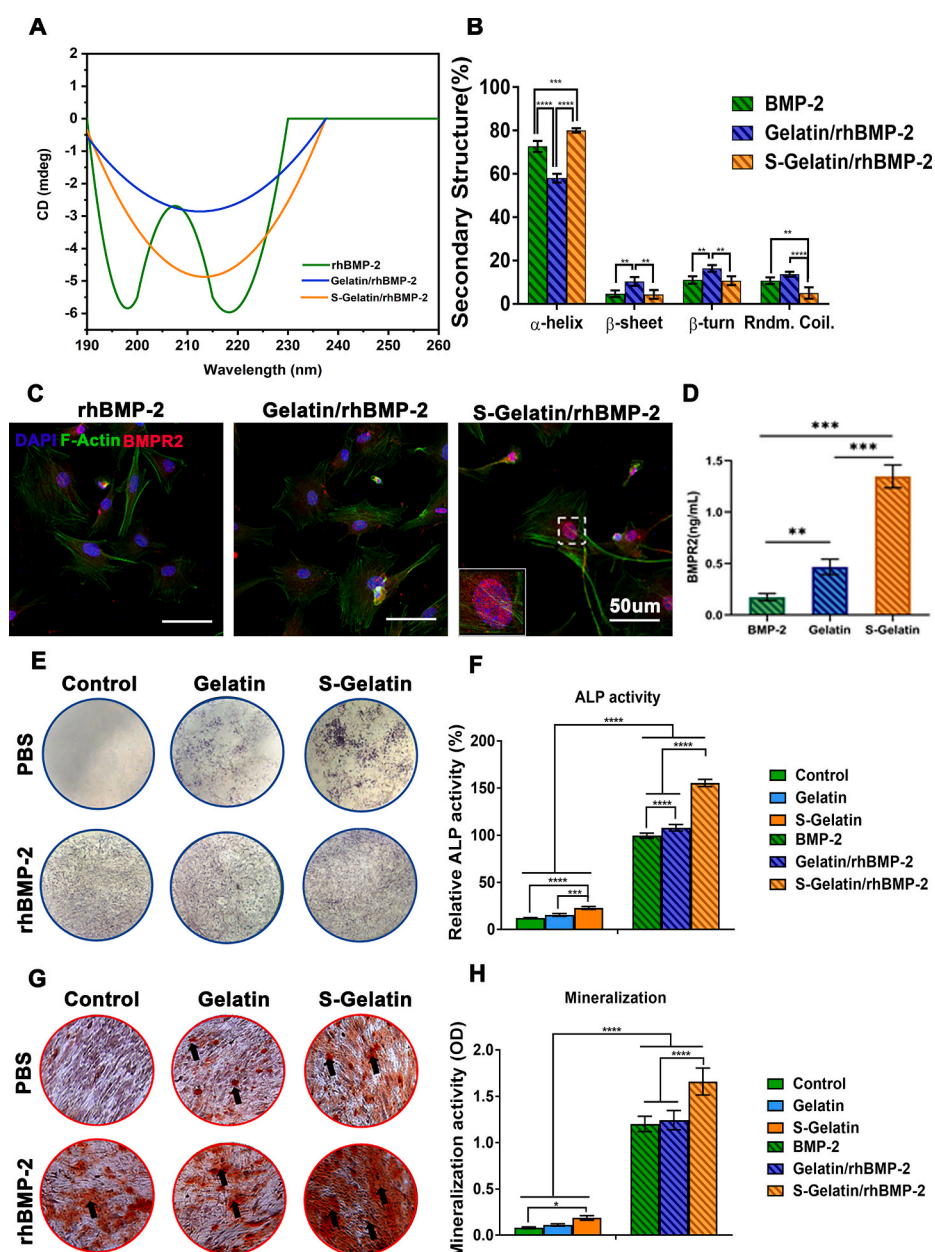
Fig. 2. BMPR2 activation on mesenchymal stem cells (MSCs) by S-Gelatin. A) Circular dichroism analysis of S-Gelatin and Gelatin to binding BMP-2. B) The quantitative analysis of binding. C) MSCs co-incubated with the hydrogels were immunostained using antibodies against BMPR2 (red) and F-actin (green) to evaluate BMPR2 activation. D) Quantitative analysis of BMPR2+ cells in each group. E) and F) Qualitative and quantitative analysis of ALP expression in treated MSCs using ALP staining assay. G) and H) Qualitative and quantitative analysis of mineralization in treated MSCs using Alizarin red staining. (*p < 0.05, **p < 0.01, ***p < 0.001, ****p < 0.0001, statistical significance when comparing each of the two groups).

charge of sulfonated gelatin and stable binding between rhBMP-2 and S-gelatin. In addition, the degradation ratio was calculated by immersing the hydrogels in the PBS, and the degradation behavior was shown in Fig. S7.It can be seen from the *in vitro* degradation experiment that both hydrogels can be completely degraded, and the degradation rate of S-Gelatin/rhBMP-2 hydrogel was faster than that of Gelatin/rhBMP-2 hydrogel due to the introduction of sulfonic acid groups as hydrophilic groups, which can increased its hydrophilicity, thereby increasing its degradation rate. Additionally, on the 7 days, the release amount is relatively close to the degradation degree of the corresponding time, indicating that the S-Gelatin/rhBMP-2 hydrogels had a significant release in the early stage, and started to release slowly after the first day with the degradation of the hydrogel until the hydrogels were completely degraded.

Thus, the sulfonated gelatin/rhBMP-2 hydrogel was successfully synthesized, and was demonstrated to efficiently bind rhBMP-2, allowing regulation of rhBMP-2 aggregation and controlled release of rhBMP-2.

3.2. Synergistic effect with rhBMP-2 via BMPR2 activation in vitro

To identify the regulation of rhBMP-2 secondary structure by sulfonated gelatin, the ultraviolet region of 190–260 nm was chosen to obtain the circular dichroism spectra, as demonstrated by Shu et al. [29] and Chen et al. [30] This ultraviolet region was selected because it reveals the most information regarding the conformation of the main chain in the biological macromolecule. As shown in Fig. 2A, with the addition of sulfonated gelatin, the double peaks of rhBMP-2 were gradually reduced and the overall shape changed to a single peak, indicating that part of the random conformation was adjusted to a regular conformation. The detailed quantitative changes in various conformations are shown in Fig. 2B [31]. The interaction of sulfonated gelatin with rhBMP-2 increased the α-helix content of rhBMP-2 by 6.67%, and decreased the random coil content by 30%, indicating that sulfonated gelatin can affect the conformation of rhBMP-2 and enhance its activity. The decreased random coil content results can enhance the BMP-2 activity as demonstrated by Sebald and Kirschy [31].Moreover, BMPR2 activation, which is reported to direct the osteogenic differentiation of stem cells, was detected on MSCs in cell culture, implying the synergistic effect of sulfonated gelatin and rhBMP-2 on osteogenesis. As shown in Fig. 2C, abundant localized puncta of BMPR2 were observed on mouse bone marrow MSCs (mBMSCs) with sulfonated gelatin; in contrast, almost no BMPR2 internalization was detected in the control and gelatin groups, demonstrating that sulfonated gelatin significantly promoted BMPR2 expression. Further, the protein content of BMPR2 in the sulphonated gelatin group was significantly higher than that in the gelatin group. Osteogenic differentiation was evaluated using both ALP staining and Alizarin red staining (ARS); the sulphonated gelatin was found to enhance ALP staining and ARS (Fig. 2E and G), demonstrating significant promotion of osteogenesis by S-gelatin/rhBMP-2, based on both ALP expression at 7 days and long-term mineralization at 14 days. As shown in Fig. 2G, sulfonated gelatin enhanced mineralization compared to the gelatin and control groups; however, with rhBMP-2 loading, S-Gelatin/rhBMP-2 enhanced mineralization significantly, demonstrating that sulfonated gelatin can synergize with rhBMP-2 to promote osteogenesis.

Collectively, the S-Gelatin/rhBMP-2 hydrogel could affect the secondary structure of rhBMP-2, stimulate BMPR2 expression in MSCs, and promote osteogenic activity via a synergistic effect with rhBMP-2 *in vitro*.

3.3. Cytokine production enhancement in vitro

MSCs can secrete different growth factors in different microenvironments. Thus, with the stimulation effect of S-Gelatin/rhBMP-2, MSCs secretion can be improved on growth factors such as OPN and OCN

related to osteogenesis as well as growth factors such as SDF-1α, FGF-2, Ang-1, and VEGF through paracrine secretion. To verify the paracrine induction of mBMSCs by S-Gelatin/rhBMP-2, an ELISA was used to measure the fundamental growth factors after mBMSCs were co-incubated with hydrogels; the same dose of rhBMP-2 was added to the medium and cultured for the same time as the control groups. After three days**,** the growth factors, including SDF-1α, FGF-2, Ang-1, VEGF, OPN, and OCN in the S-Gelatin/rhBMP-2 group were significantly more abundant than those in the gelatin and rhBMP-2 groups (Fig. 3A–F). Among the upregulated factors, SDF-1α and FGF-2 were significantly higher in the sulfonated gelatin group than in the gelatin and rhBMP-2 groups, indicating that sulfonated gelatin loaded with rhBMP-2 exhibited better potential to induce stem cell recruitment and proliferation and that SDF-1α and FGF-2 are important growth factors in the recruitment and proliferation of stem and progenitor cells. Further, upregulated growth factors, such as Ang-1 and VEGF, indicated better angiogenic potential, and the highly expressed OPN and OCN indicated better osteogenic potential.

Together, the S-Gelatin/rhBMP-2 hydrogel can induce MSCs to secrete multiple growth factors such as SDF-1α, FGF-2, Ang-1, VEGF, OPN, and OCN, indicating that the S-Gelatin/rhBMP-2 hydrogel has good potential for improving cell proliferation, osteogenesis, and vascularization.

### 3.4. Multi-growth factor enrichment and BMPR2 activation in vivo

As the S-Gelatin/rhBMP-2 hydrogel can induce the production of various growth factors *in vitro*, we measured fundamental growth factors in the gelatin and sulfonated gelatin groups using ELISA *in vivo*; the concentrations of growth factors in the femur were used as controls. At nearly 28 days**,** the growth factors, including VEGF, FGF-2, SDF-1a, OPG, OPN and RANK in the sulfonated gelatin group were significantly higher than those in the gelatin group and femur, as suggested by Fig. 4A–F and Fig. S6. In particular, the SDF concentration after 3 days in the sulfonated gelatin group was approximately 1.5 times that in the other groups, indicating that it had a good potential in recruiting stem cells and progenitor cells. Further, upregulated growth factors such as Ang-1 and VEGF indicated better angiogenic potential, and highly expressed OPG and OPN demonstrated better osteogenic potential.

Furthermore, BMPR2 activation *in vivo* was determined using immunofluorescence. As shown in Fig. 4G, the fluorescence intensity of BMPR2 in the S-Gelatin/rhBMP-2 hydrogel was significantly stronger than that in the gelatin group. However, the low expression of BMPR2 on day 7 indicated that BMPR2 signaling was completed and that the downstream processes were underway as demonstrated by Sánchez-Duffhues et al. [32] and Drake et al. [33].

In summary, the S-Gelatin/rhBMP-2 hydrogel can promote the expression of various growth factors *in vivo,* among which, upregulated SDF-1α and FGF-2 could promote the recruitment and proliferation of stem cells and progenitor cells, whereas other growth factors could promote osteogenesis and angiogenesis via BMPR2 activation.

3.5. Stem cell recruitment in vivo

As the S-Gelatin/rhBMP-2 hydrogel can enhance the expression of SDF-1α and FGF-2 *in vivo*, the recruitment of SDF-1α-sensitive cells, such as MSCs, was mainly investigated (Fig. 5). Flow cytometry analysis was used to analyze the MSC content *in vivo*. As shown in Fig. 5A–D, the content of MSCs in the S-Gelatin/rhBMP-2 hydrogel reached a peak at 7 days, accounting for 1.3% of the total cell mass, and their ratio was twice that in the gelatin group, indicating that the S-Gelatin/rhBMP-2 hydrogel can recruit more MSCs *in vivo*(The gate selection was shown in Fig. S10). However, at 14 days, the content of MSC in S-Gelatin/rhBMP-2 hydrogel began to decrease while the content of MSC in Gelatin/rhBMP-2 hydrogel was still increasing, however, the content of MSC in S-Gelatin/rhBMP-2 hydrogel was significantly higher than Gelatin/
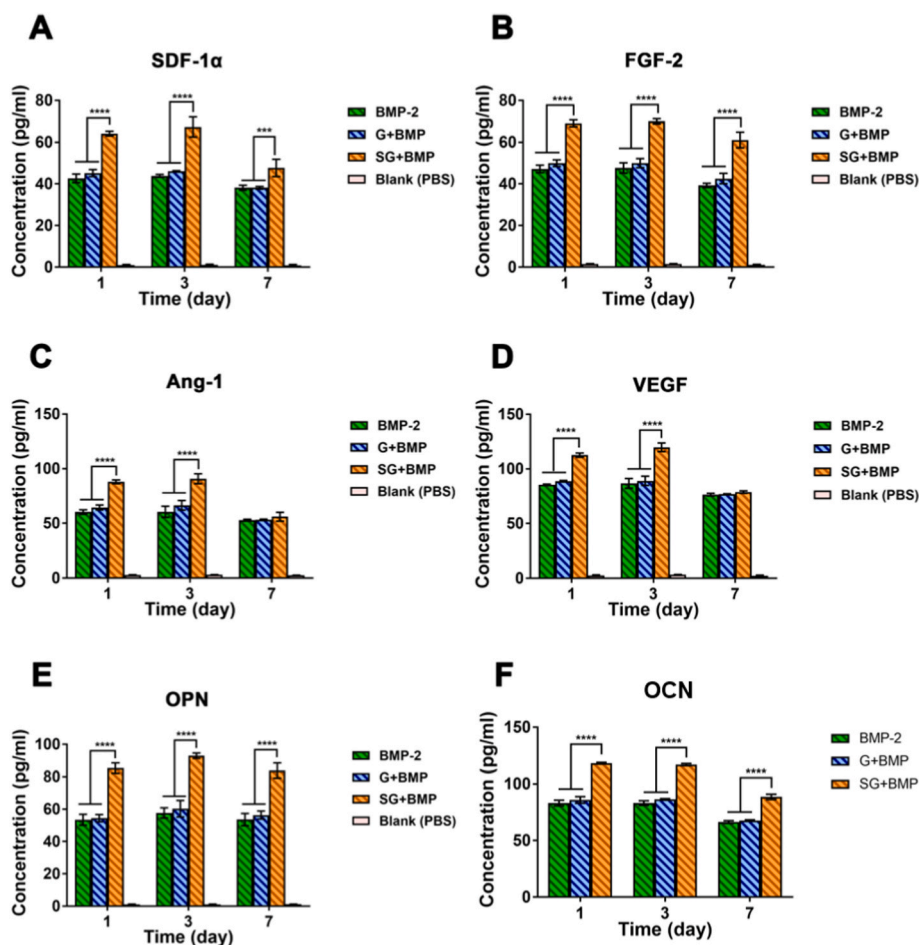
Fig. 3. The cytokine production by MSCs *in vitro*. Quantitative analysis of A) SDF-1α, B) FGF-2, C) Ang-1, D) VEGF, E) OPN, and G) OCN expression in MSCs cultured with various treatments for 7 days. MSCs treated with S-Gelatin/rhBMP-2 hydrogels presented a significant increase in almost all growth factors during the culture. (*p < 0.05, **p < 0.01, ***p < 0.001, ****p < 0.0001, statistical significance upon comparing each of the two groups).

rhBMP-2 group, indicating that the S-Gelatin/rhBMP-2 hydrogel could recruit more MSCs quickly. Furthermore, the content of MSCs in the S-Gelatin/rhBMP-2 hydrogel decreased faster than in the gelatin group during 14 days to 28days, indicating that MSCs in S-Gelatin/rhBMP-2 showed better potential for differentiation. Immunofluorescence staining was used to further characterize the MSCs in S-Gelatin/rhBMP-2 and gelatin/rhBMP-2. As shown in Fig. 5E, at 7 and 14 days, the population of MSCs in the S-Gelatin/rhBMP-2 group was significantly higher than that in the gelatin group, and its distribution in the sulfonated gelatin group was relatively aggregated. Furthermore, the mechanical properties of hydrogels showed dramatic effects on cell behavior during stem cell recruitment, and the strain-stress curve was calculated by Universal testing machine. As shown in Fig. S5, with the introduction of sulfonic acid groups, the stiffness of the molecular chain was slightly increased, which affects the mechanical strength of the hydrogel, however, there was no significant difference in the strength and Young's modulus of the gelatin and S-Gelatin hydrogel, indicated the mechanical properties had no effect on cell behavior during the *in situ* construction of GEMs.

In addition, along with the recruitment of stem cells, the recruitment of immune cells by S-Gelatin/rhBMP-2 hydrogels is also a non-negligible part. Flow cytometry was used to analyze the recruitment effect of different hydrogels on macrophages, B cells and T cells at different time points. As shown in Fig. S11, at 7 days, the content of macrophages in S-Gelatin/rhBMP-2 hydrogels was three times than that of Gelatin/rhBMP-2, and was significantly higher than the femur group, however, at 14 days, the content of macrophages in S-Gelatin/rhBMP-2 was comparable to that of macrophages in the femur. Additionally, the

recruitment effect of different hydrogels on T cells exhibited the same trend as macrophages as shown in Figs. S11E–H.

Altogether, S-Gelatin/rhBMP-2 recruits MSCs faster and in greater numbers compared with gelatin/rhBMP-2; further the MSCs in the sulfonated gelatin group show better differentiation potential.

3.6. Vascularization in vitro

With the induction of a large amount of VEGF and Ang-1, as well as stem cell recruitment into the S-Gelatin/rhBMP-2 hydrogel, the potential for vascular regeneration was naturally concentrated. RT-PCR, FACs, and immunohistochemical analyses were performed to examine this aspect. To determine the changes in angiogenesis, two important genes for vascularization, *Ang-1* and *Vegf*, were analyzed using qRT-PCR. As shown in Fig. 6A, upregulation of *Ang-1* and *Vegf* in the S-Gelatin/rhBMP-2 group compared to the gelatin group and the femur, reconfirmed that S-Gelatin/rhBMP-2 can upregulate angiogenesis-related gene expression.

As shown in Fig. 6B, CD31 positive endothelial cells were gradually recruited into the hydrogels. Significantly more blood vessel-related cells were recruited to the S-Gelatin/rhBMP-2 hydrogels than to the gelatin group at 7 days. At 14 days, the sulfonated gelatin recruited more CD31 positive endothelial cells. Furthermore, endothelial progenitor cells, which are important cells in blood vessel formation, were analyzed to investigate vascularization and angiogenesis. As shown in Fig. 6C and Fig. S9, S-Gelatin/rhBMP-2 had significantly larger numbers of αEPCs than both the femur and gelatin/rhBMP-2 groups. The content of αEPCs
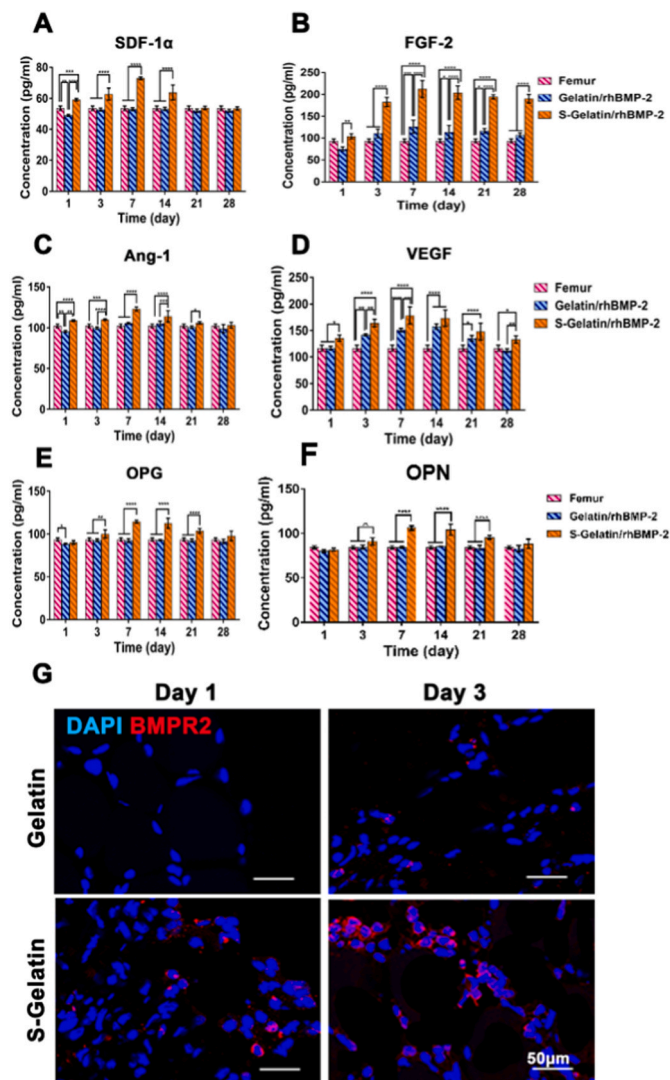
Fig. 4. Chemotactic factor expression *in vivo*. Quantitative analysis of A) SDF-1α, B) FGF-2, C) Ang-1, D) VEGF, E) OPN, and G) RANK expressed *in vivo* with various treatments for 28 days. The S-Gelatin/rhBMP-2 group presented a significant increase in almost all growth factors over the long-term. (*p < 0.05, **p < 0.01, ***p < 0.001, ****p < 0.0001, statistical significance when comparing each of the two groups). G) The cells aggregated in hydrogels were immunostained using antibodies against BMPR2 (red) and DAPI (blue) to evaluate BMPR2 activation *in vivo*.

recruited by the sulfonated gelatin was four times higher than that in the gelatin group at 7 days, indicating that S-Gelatin/rhBMP-2 exhibited better potential for vascularization.

Finally, immunohistochemical staining for CD31 was used to visualize the blood vessel formation induced by the hydrogels. As shown in Fig. 6D, large amounts of CD31-positive cells were recruited to the S-Gelatin/rhBMP-2 at 7 days; further, the CD31-positive cells gradually formed a ring structure, suggesting the formation of blood vessels at 14 days.

3.7. Enhanced bone formation in vivo

With the induction of a large amount of RANK and OPG, as well as MSC recruitment into the S-Gelatin/rhBMP-2 hydrogel, bone tissue formation was evaluated using an ectopic osteogenesis model generated in mouse hind limb muscle pockets as demonstrated by Liu et al. [30] and Nakamuru et al. [34] Safranin O-Fast Green was used to assess the ectopic bone formation. As shown in Fig. 7A, at week 1, a large number

of chondrogenic cells were observed in the S-Gelatin/rhBMP-2 group, whereas the gelatin/rhBMP-2 group showed only a few chondrocyte nuclei. Further, the S-Gelatin/rhBMP-2 group showed accelerated bone generation at week 2; in contrast, trabecular bone formation in the gelatin/rhBMP-2 group was clearly less pronounced, indicating that sulfonated gelatin accelerated rhBMP-2-induced cartilage and bone formation. As suggested in a previous study, lack of biomechanical regulation and sustained stimulation with exogenous rhBMP-2, bone resorption was observed in the ectopic bones along with extensive adipogenesis as demonstrated by the Safranin O-Fast Green in the gelatin group at 28 days. However, the S-Gelatin/rhBMP-2 hydrogel inhibited adipogenesis, as shown by Safranin O-Fast Green staining in the sulfonated gelatin group after 28 days. Furthermore, previous studies have demonstrated that the TGF-β/Smad signaling pathway can mediate osteogenic differentiation via BMPR2 activation; therefore, we focused on the TGF-β/Smad signaling pathway and verified whether the synergistic effect of sulfonated gelatin and BMP-2 was mediated by this signaling pathway. As shown in Fig. 7B and C, important genes in the TGF-β/Smad signaling pathway, including *Bmpr2, Smad 1, Smad 4, Runx2*, and *Opn* were increased in the S-Gelatin/rhBMP-2 group. The highly significant expression patterns in the S-Gelatin/rhBMP-2 group and femur are shown as a volcano plot in Fig. 7C.

Furthermore, qRT-PCR and western blotting were used to further verify the expression of key genes and proteins in the TGF-β/Smad signaling pathway, respectively. As shown in Fig. 7E, the expression of *Bmpr2, Smad1,* and *Smad4* in the sulfonated gelatin group was significantly higher than that in the femur and gelatin groups, indicating that sulfonated gelatin loaded with rhBMP-2 can promote osteogenic differentiation via the TGF-β/Smad signaling pathway. In addition, as shown in Fig. 7F, the S-Gelatin/rhBMP-2 hydrogel significantly upregulated the expression of Smad4 and its downstream proteins, Runx2 and OPN.

In conclusion, the S-Gelatin/rhBMP-2 hydrogel can accelerate rhBMP-2 induced osteogenesis via the TGF-β/Smad signaling pathway.

4. Discussion

Bone fractures and defects, still account for more than 1 million patients hospitalized annually in the United States, of which 5–10% cases are complicated by delayed healing or nonunion, thus posing a major clinical challenge [35,36]. As a generally assumed osteoinductive cue for bone development and healing, BMP-2 is widely used in the clinic because of its high efficacy in osteogenesis induction [37]. However, *in situ* BMP-2 therapy for bone repair is still in preliminary stages and faces many challenges, including the short half-life of BMP-2 protein, metabolic clearance *in vivo*, and the need for continuous osteogenic stimulation for efficacious bone regeneration [38,39]. Considering the critical role of biomaterial-based BMP-2 strategies to assist the secretion of endogenous growth factors in the regulation of osteogenesis behavior as well as activation of the BMP-2 receptor and downstream pathway for bone regeneration, we introduced an S-Gelatin hydrogel to induce a growth factor-enriched microenvironment *in situ* and thus recapitulate and accelerate the osteogenesis process; this hydrogel not only overcame the drawbacks resulting from the limitation of external factors and cell incorporation, but also induced better osteogenesis compared to traditional BMP-2 delivering biomaterials. To our knowledge, this is the first study to demonstrate a biomaterial with a combination of endogenous growth factor enrichment design and BMPR2 activation, offering a promising alternative strategy and novel biomaterial design for BMP-2 therapy in bone regeneration.

BMPR2 is widely known as an essential signal for modulating the genes involved in osteogenesis [40–42]. Although substantial coupling between exogenous growth factors and cells has been demonstrated [43], the synergistic effect of BMPR2 activation with the establishment of a growth factor-enriched microenvironment remains elusive and is highly desirable, especially for long-term treatment of bone defects.
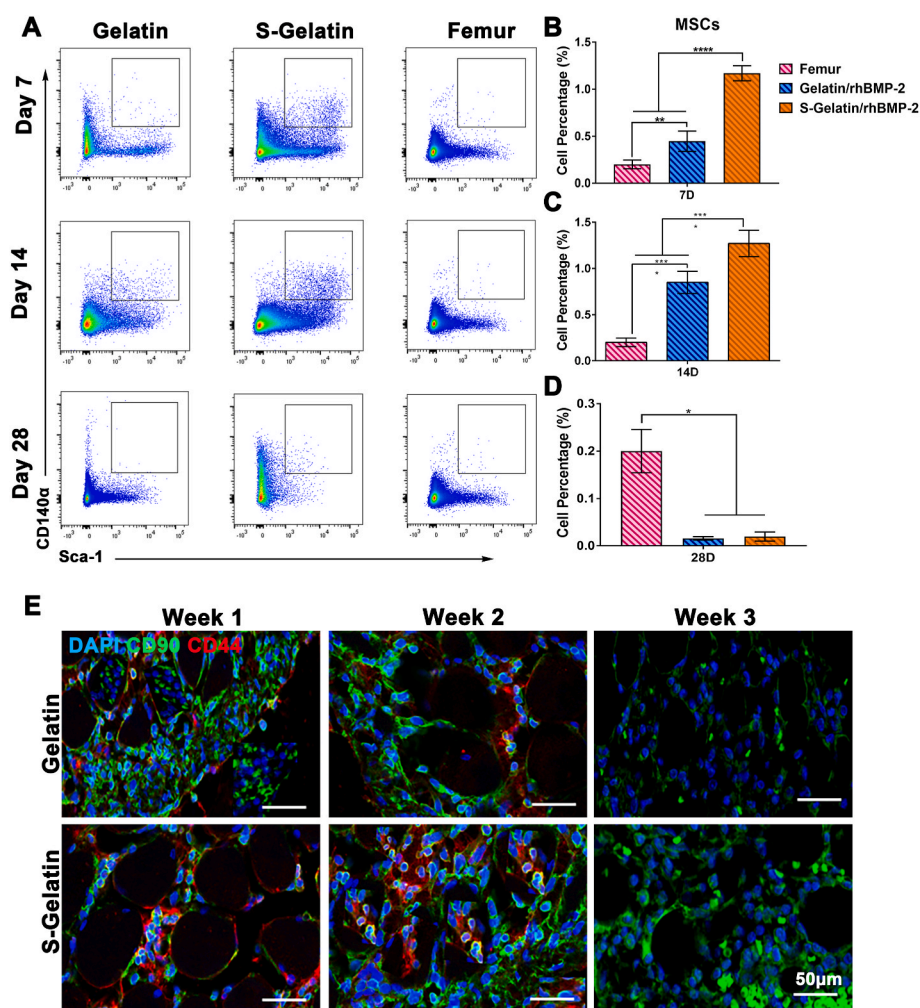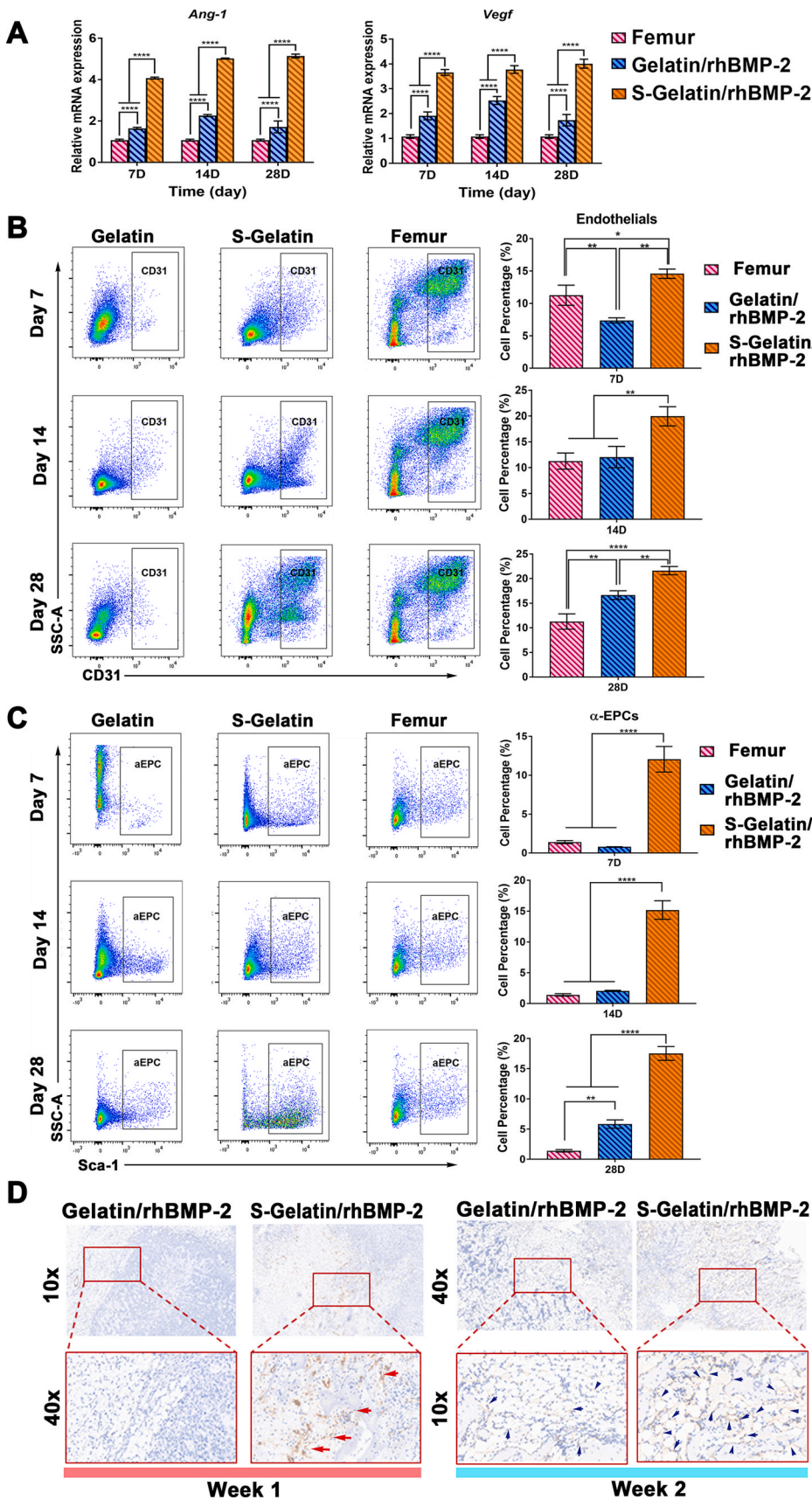
Fig. 5. Recruitment of MSCs by hydrogels *in vivo*. A) Flow cytometric analysis of MSCs in the Femur, Gelatin/rhBMP-2, and S-Gelatin/rhBMP-2 for 28 days. The MSCs were gated as $CD31^-CD140a^+Sca-1^+$ cells. The quantitative analysis of MSC percentages in different groups at B) Day 7, C) Day 14, and D) Day 28. The percentage of MSCs in S-Gelatin/rhBMP-2 was significantly higher than that in the other two treatments in the early stage, but sharply dropped at Day 28 (*$p < 0.05$, **$p < 0.01$, ***$p < 0.001$, ****$p < 0.0001$, statistical significance when comparing each of the two groups). E) Tissues around the hydrogels were immunostained using antibodies against CD44 (red) and CD90 (green) to identify mBMSCs recruited *in vivo* at 2 weeks. Nuclei were stained with DAPI (blue).

Previously, a novel hydrogel composed of gelatin and sulfonated chitosan was reported to improve VEGF levels by controlling macrophage secretion [44,45]. However, the introduction of single or dual growth factors into the bone defect area is inevitably monotonous and inadequate to form the complex microenvironment during repair *in vivo*, which requires development with various pathophysiological processes [46,47]. Unlike strategies with a simple combination of exogenous molecules or cells, the BMP-2-incorporated S-Gelatin hydrogel described in this study could establish a growth factor-mimicking microenvironment to harness the osteoinductivity of the BMPR2-Smad-OPN pathway via BMPR2 activation in MSCs and its binding with BMP-2. In our study, BMP-2 was incorporated into the S-gelatin hydrogels, which endowed the system with a suitable molecule release design for complicated bone regeneration. After crosslinking and fabrication, BMP2 was well-distributed in the S-Gelatin/rhBMP-2 hydrogel and prolonged release was achieved by hydrogel degradation control (as shown in Fig. 1D and E), implying a homogenous structure and an improved microenvironment *in vivo*. More specifically, with the incorporation of S-Gelatin, receptor utilization of BMP-2 signals was enhanced via BMPR2 activation (Fig. 2), which was beneficial to the osteogenic differentiation of MSCs and subsequent osteogenic activities [48,49]. As for the receptor stimulation capacity, S-Gelatin/rhBMP-2 exhibited a 10-fold and 8-fold increase in BMPR2 expression compared to the direct BMP-2 treatment (Figs. 2A and 4G) *in vitro* and *in vivo*, respectively, which achieved increased ALP activity and mineralization, reinforcing the osteogenic differentiation of MSCs. Additionally, cytokine secretion by MSCs was induced and a microenvironment with multiple growth factors was achieved, which partially mimicked the growth factor components in the stem cell niche, which favors organogenesis and tissue regeneration [50–52]. As a result of the stimulation capability of cytokine secretion, the growth factors in S-Gelatin/rhBMP-2, including SDF-1α, Ang-1, VEGF, and RANK, were increased significantly compared to those in the gelatin/rhBMP-2 and bare BMP-2 treatments (Figs. 3 and 4) *in vitro* and *in vivo*, demonstrating enrichment of endogenous growth factors to accelerate tissue regeneration. Taken together, S-Gelatin/rhBMP-2 hydrogels with a BMP-2/BMPR2 synergistic effect can stably increase osteogenesis activity through a collection of endogenous growth factors to modulate MSC behavior for driving bone regeneration.

Concerning the cellular and molecular levels *in vitro* and *in vivo*, S-Gelatin/rhBMP-2 hydrogels significantly promoted the recruitment of MSCs, $CD31^+$ endothelial cells, and α-EPCs, which are involved in tissue repair (Figs. 5 and 6), via growth factor induction; further, these hydrogels facilitated the differentiation of MSCs and their maturation (Fig. 7A, B, and D). According to the analysis of *in vivo* vascularization, S-Gelatin/rhBMP-2 hydrogel stimulated *Vegf* and *Ang-1* gene expression and demonstrated the recruitment of $CD31^+$ endothelial cells, which is an important index for blood vessel formation. Conversely, gelatin/rhBMP-2 showed almost no CD31 deposition at 1 week and only a small amount during the study period. Based on the advanced improvement in the cellular and tissue levels, osteogenesis was evaluated *in vivo* using an ectopic bone model; the results confirmed that more chondrocytes presented in S-Gelatin/rhBMP-2 hydrogels than in the gelatin/rhBMP-2 hydrogels at 1 week with significantly accelerated ossification over a longer period. In addition, the S-Gelatin/rhBMP-2

Fig. 6. Vascularization activity induced by hydrogels *in vivo*. A) The gene expression of *Ang-1* and *Vegf* in the Femur, Gelatin/rhBMP-2, and S-Gelatin/rhBMP-2. B) Flow cytometric analysis of endothelial cells in the Femur, Gelatin/rhBMP-2, and S-Gelatin/rhBMP-2 groups for 28 days. The endothelial cells were gated as CD31+ cells. The quantitative analysis of endothelial cell percentages in different groups at various time points is shown at the right side, respectively. C) Flow cytometric analysis of α-endothelial progenitor cells (α-EPCs) in the Femur, Gelatin/rhBMP-2, and S-Gelatin/rhBMP-2 groups for 28 days. The α-EPCs were sorted from CD31+ endothelial cells in B) and further gated as CD31+ Sca-1+ cells. The quantitative analysis of α-EPCs in different groups from various time points is shown at the right side, respectively. The α-EPC percentages in S-Gelatin/rhBMP-2 were significantly higher than those in other two treatments throughout the experiment. (*$p < 0.05$, **$p < 0.01$, ***$p < 0.001$, ****$p < 0.0001$, statistical significance when comparing each of the two groups). D) Immunohistochemical analysis for CD31-positive cells in and around hydrogels *in vivo*. The CD31 depositions were dark red with red/blue arrows labeled in slices at Week 1 and Week 2. CD31 staining was evidently increased in S-Gelatin/rhBMP-2 compared with that in Gelatin/rhBMP-2.
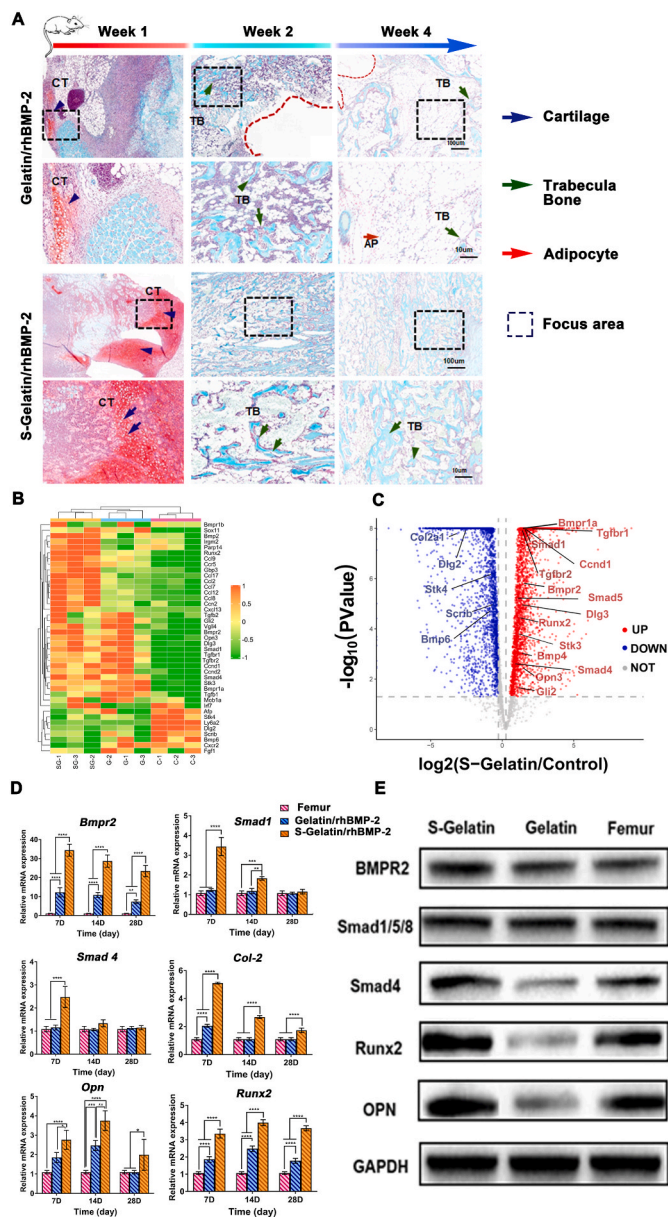
Fig. 7. Osteogenesis activity induced by hydrogels *in vivo*. A) Histological staining of tissues formed by hydrogel induction using Safranin O-Fast Green (2 magnifications) at Week 1, 2, and 4. There were obviously more chondrogenic cells surrounding the S-Gelatin/rhBMP-2 hydrogels based on safranin O staining at Week 1, which were quickly ossified into trabecular bones with time. The enlarged view of trabecular bone or chondrogenic cells was amplified from the areas enclosed by the dash-lined frames. Blue arrows: cartilage; Green arrows: trabecular bone; Red arrows: adipocytes. B) differentially expressed gene(DEG) profiling for the selected genes regulated by hydrogels from A). C) A volcano plot of DEGs revealed the fold-changes of the selected genes between the S-Gelatin/rhBMP-2 and Femur groups. D) Relative mRNA expression of tissues formed by hydrogel induction in A). E) Qualitative analysis of BMPR2, Smad1/5/8, Smad4, Runx2, and Opn protein expression in the formed tissue in A) using western blot.

group showed more mineralized bone than the gelatin/rhBMP-2 group from 2 to 4 weeks, and ultimately reached optimal osteogenesis at 4 weeks. Focusing on the regulation mechanism of osteogenesis promotion, activation of the BMPR2/intracellular Smad pathway, which mediate osteogenic differentiation-related gene transcription [53], was examined; the pathway components were significantly upregulated in the S-gelatin/rhBMP-2 group, as shown in Fig. 7E and F.

Altogether, these results are the first indication that a S-Gelatin/rhBMP-2 hydrogel could trigger multiple endogenous growth factors to establish a complex cell niche for bone healing. Moreover, combined with BMPR2 activation, the bone reconstruction in the present study seems to be more biomimetic; therefore, this growth factor-enrichment biomaterial strategy for niche achievement and efficient bone tissue regeneration is highly intriguing.

Based on the described advantages, programming of the endogenous growth factor microenvironment and harmonious bone regeneration through S-Gelatin/rhBMP-2 hydrogel can be achieved via two mechanisms: the BMPR2/Smad downstream pathway and endogenous growth factor induction. First, S-Gelatin/rhBMP-2 hydrogel-induced BMPR2 activation greatly contributed to the utilization of BMP-2 for MSC differentiation and osteogenesis. In agreement with published studies [40, 54], the S-gelatin/rhBMP-2 hydrogels induced stem cell differentiation into osteogenic cells via activation of a BMPR2/Smad/Opn downstream pathway and upregulation of osteogenic markers such as OPN, Col-2, and RANK. Second, the induction of cytokine secretion by MSCs resulted in favorable endogenous growth factor localization and formed a niche *in situ* via the homing of MSCs and endothelial cells during the regeneration stage. Migration of MSCs to damaged sites and the induction of growth factors to form a regenerating microenvironment is known to be critical for tissue repair [55–57]. Consistent with these reports, we found that the endogenous growth factor enrichment induced by S-Gelatin/rhBMP-2 could effectively regulate stem cell behaviors, including promoted migration and differentiation of MSCs, maturation of endothelial progenitor cells, and vascularization of CD31^{+} endothelial cells.

Therefore, the abundant growth factor enhancement induced by S-Gelatin/BMP2 spontaneously achieved osteogensis and recapitulated a stem cell niche for promoting bone regeneration.

5. Conclusion

In summary, the present study demonstrated a novel hydrogel combining sulfonated gelatin and rhBMP-2 to amplify BMP-2 signaling and further recapitulate the *in situ* growth factor-abundant microenvironment via regulation of varies biological and physical processes involved in bone regeneration. Specifically, S-Gelatin/rhBMP-2 with BMP receptor activation had a striking effect on MSC response and cytokine secretion promotion, enriching endogenous growth factors for *in vivo* bone regeneration. This study also provides strong evidence that MSC behaviors, including growth factor secretion, cell recruitment, and differentiation, can be dramatically induced and modulated using sulfonated hydrogels/rhBMP-2, achieving a suitable stem cell niche to accelerate ossification and thereby approach efficient bone regeneration. Our findings may have significant implications for understanding biomaterial-induced biological effects as well as bone regeneration challenged by aging and osteoporosis. In the future, to determine the effect of the S-Gelatin/rhBMP-2 hydrogels on tissue repair under abnormal conditions, more studies need to be done on standardized models in aging or diseases, which may further clarify the regeneration mechanisms and direct the applications of the hydrogel.

Ethics approval

All surgical procedures were approved by the Institutional Animal Care and Use Committee of East China University of Science and Technology.

CRediT authorship contribution statement

Qinghao Zhang: Conceptualization, Methodology, Investigation, Data curation, Writing – original draft, Writing – review & editing. **Yuanda Liu:** Methodology, Investigation, Software, Data curation, Writing – original draft. **Jie Li:** Investigation, Software. **Jing Wang:**

Conceptualization, Methodology, Writing – review & editing, Supervision, Funding acquisition. **Changsheng Liu:** Conceptualization, Supervision, Funding acquisition.

Declaration of competing interest

The authors declare no conflicts of interest.

Acknowledgements

Appendix A. Supplementary data

Supplementary data to this article can be found online at https://doi.org/10.1016/j.bioactmat.2022.06.012.

References

[1] S.H. Lee, H. Shin, Matrices and scaffolds for delivery of bioactive molecules in bone and cartilage tissue engineering, Adv. Drug Del. Rev. 59 (2007) 339–359, https://doi.org/10.1016/j.addr.2007.03.016.

[2] A. Ho-Shui-Ling, J. Bolander, L.E. Rustom, A.W. Johnson, F.P. Luyten, C. Picart, Bone regeneration strategies: engineered scaffolds, bioactive molecules and stem cells current stage and future perspectives, Biomaterials 180 (2018) 143–162, https://doi.org/10.1016/j.biomaterials.2018.07.017.

[3] S.D. Subramony, B.R. Dargis, M. Castillo, E.U. Azeloglu, M.S. Tracey, A. Su, H.H. Lu, The guidance of stem cell differentiation by substrate alignment and mechanical stimulation, Biomaterials 34 (2013) 1942–1953, https://doi.org/10.1016/j.biomaterials.2012.11.012.

[4] C.A. Dumitru, H. Hemeda, M. Jakob, S. Lang, S. Brandau, Stimulation of mesenchymal stromal cells (MSCs) via TLR3 reveals a novel mechanism of autocrine priming, The FASEB J 28 (2014) 3856–3866, https://doi.org/10.1096/fj.14-250159.

[5] E. Mooney, J.N. Mackle, D.J.P. Blond, E. O`Cearbhaill, G. Shaw, W.J. Blau, F.P. Barry, V. Barron, J.M. Murphy, The electrical stimulation of carbon nanotubes to provide a cardiomimetic cue to MSCs, Biomaterials 33 (2012) 6132–6139, https://doi.org/10.1016/j.biomaterials.2012.05.032.

[6] P.J. Marie, Bone cell senescence: mechanisms and perspectives, J. Bone Miner. Res. 29 (2014) 1311–1321, https://doi.org/10.1002/jbmr.2190.

[7] P.J. Marie, Targeting integrins to promote bone formation and repair, Nat. Rev. Endocrinol. 9 (2013) 288–295, https://doi.org/10.1038/nrendo.2013.4.

[8] H. Lin, J. Sohn, H. Shen, M.T. Langhans, R.S. Tuan, Bone marrow mesenchymal stem cells: aging and tissue engineering applications to enhance bone healing, Biomaterials 203 (2019) 96–110, https://doi.org/10.1016/j.biomaterials.2018.06.026.

[9] J.V. Chakkalakal, K.M. Jones, M.A. Basson, A.S. Brack, The aged niche disrupts muscle stem cell quiescence, Nature 490 (2012) 355–360, https://doi.org/10.1038/nature11438.

[10] Y. Kfoury, D.T. Scadden, Mesenchymal cell contributions to the stem cell niche, Cell Stem Cell 16 (2015) 239–253, https://doi.org/10.1016/j.stem.2015.02.019.

[11] B.C. Lee, K.R. Yu, Impact of mesenchymal stem cell senescence on inflammaging, BMB Rep 53 (2020) 65–73, https://doi.org/10.5483/BMBRep.2020.53.2.291.

[12] F.Z. Asumda, Age-associated changes in the ecological niche: implications for mesenchymal stem cell aging, Stem Cell Res. Ther. 4 (2013) 47, https://doi.org/10.1186/scrt197.

[13] E.R. Balmayor, J.P. Geiger, C. Koch, M.K. Aneja, M. van Griensven, C. Rudolph, C. Plank, Modified mRNA for BMP-2 in combination with biomaterials serves as a transcript-activated matrix for effectively inducing osteogenic pathways in stem cells, Stem Cell. Dev. 26 (2016) 25–34, https://doi.org/10.1089/scd.2016.0171.

[14] D.S. Bramono, S. Murali, B. Rai, L. Ling, W.T. Poh, Z.X. Lim, G.S. Stein, V. Nurcombe, A.J. van Wijnen, S.M. Cool, Bone marrow-derived heparan sulfate potentiates the osteogenic activity of bone morphogenetic protein-2 (BMP-2), Bone 50 (2012) 954–964, https://doi.org/10.1016/j.bone.2011.12.013.

[15] M.G.L. Olthof, L. Lu, M.A. Tryfonidou, L.D. Loozen, B. Pouran, M.J. Yaszemski, B.P. Meij, W.J.A. Dhert, J. Alblas, D.H.R. Kempen, The osteoinductive effect of controlled bone morphogenic protein 2 release is location dependent, Tissue Eng. Pt. A. 25 (2018) 193–202, https://doi.org/10.1089/ten.tea.2017.0427.

[16] W. He, Q. Wang, X. Tian, G. Pan, Recapitulating dynamic ECM ligand presentation at biomaterial interfaces: molecular strategies and biomedical prospects, Exploration 2 (2022), 20210093, https://doi.org/10.1002/EXP.20210093.

[17] S. Trujillo, C. Gonzalez-Garcia, P. Rico, A. Reid, J. Windmill, M.J. Dalby, M. Salmeron-Sanchez, Engineered 3D hydrogels with full-length fibronectin that sequester and present growth factors, Biomaterials 252 (2020), https://doi.org/10.1016/j.biomaterials.2020.120104, 120104.

[18] W. He, J. Bai, X. Chen, D. Suo, S. Wang, Q. Guo, W. Yin, D. Geng, M. Wang, G. Pan, X. Zhao, B. Li, Reversible dougong structured receptor–ligand recognition for building dynamic extracellular matrix mimics, Proc. Natl. Acad. Sci. U. S. A. 119 (2022), e2117221119, https://doi.org/10.1073/pnas.2117221119.

[19] Contents: (adv. Funct. Mater. 24/2021, Adv. Funct. Mater. 31 (2021), 2170172, https://doi.org/10.1002/adfm.202170172.

[20] C. Zheng, J. Chen, S. Liu, Y. Jin, Stem cell-based bone and dental regeneration: a view of microenvironmental modulation, Int. J. Oral Sci. 11 (2019) 23, https://doi.org/10.1038/s41368-019-0060-3.

[21] B.D. Sui, C.H. Hu, A.Q. Liu, C.X. Zheng, K. Xuan, Y. Jin, Stem cell-based bone regeneration in diseased microenvironments: challenges and solutions, Biomaterials 196 (2019) 18–30, https://doi.org/10.1016/j.biomaterials.2017.10.046.

[22] H. Xia, X. Li, W. Gao, X. Fu, R.H. Fang, L. Zhang, K. Zhang, Tissue repair and regeneration with endogenous stem cells, Nat. Rev. Mater. 3 (2018) 174–193, https://doi.org/10.1038/s41578-018-0027-6.

[23] A.R. Sas, K.S. Carbajal, A.D. Jerome, R. Menon, C. Yoon, A.L. Kalinski, R.J. Giger, B.M. Segal, A new neutrophil subset promotes CNS neuron survival and axon regeneration, Nat. Immunol. 21 (2020) 1496–1505, https://doi.org/10.1038/s41590-020-00813-0.

[24] J.E. Won, Y.S. Lee, J.H. Park, J.H. Lee, Y.S. Shin, C.H. Kim, J.C. Knowles, H.W. Kim, Hierarchical microchanneled scaffolds modulate multiple tissue-regenerative processes of immune-responses, angiogenesis, and stem cell homing, Biomaterials 227 (2020), https://doi.org/10.1016/j.biomaterials.2019.119548, 119548.

[25] E. Chen, L. Yang, C. Ye, W. Zhang, J. Ran, D. Xue, Z. Wang, Z. Pan, Q. Hu, An asymmetric chitosan scaffold for tendon tissue engineering: in vitro and in vivo evaluation with rat tendon stem/progenitor cells, Acta Biomater. 73 (2018) 377–387, https://doi.org/10.1016/j.actbio.2018.04.027.

[26] L. Huang, M. Shen, G.A. Morris, J. Xie, Sulfated polysaccharides: immunomodulation and signaling mechanisms, Trends Food Sci. Technol. 92 (2019) 1–11, https://doi.org/10.1016/j.tifs.2019.08.008.

[27] A. Liu, D. Lin, H. Zhao, L. Chen, B. Cai, K. Lin, S.G.F. Shen, Optimized BMSC-derived osteoinductive exosomes immobilized in hierarchical scaffold via lyophilization for bone repair through Bmpr2/Acvr2b competitive receptor-activated Smad pathway, Biomaterials 272 (2021), https://doi.org/10.1016/j.biomaterials.2021.120718, 120718.

[28] C. Zhao, X. Wang, L. Gao, L. Jing, Q. Zhou, J. Chang, The role of the micro-pattern and nano-topography of hydroxyapatite bioceramics on stimulating osteogenic differentiation of mesenchymal stem cells, Acta Biomater. 73 (2018) 509–521, https://doi.org/10.1016/j.actbio.2018.04.030.

[29] Y. Shu, Y. Yu, S. Zhang, J. Wang, Y. Xiao, C. Liu, The immunomodulatory role of sulfated chitosan in BMP-2-mediated bone regeneration, Biomater. Sci. 6 (2018) 2496–2507.

[30] R. Chen, J. Wang, C. Liu, Biomaterials act as enhancers of growth factors in bone regeneration, Adv. Funct. Mater. 26 (2016) 8810–8823, https://doi.org/10.1002/adfm.201603197.

[31] T. Kirsch, W. Sebald, M.K. Dreyer, Crystal structure of the BMP-2–BRIA ectodomain complex, Nat. Struct. Biol. 7 (2000) 492–496, https://doi.org/10.1038/75903.

[32] G. Sánchez-Duffhues, A. García de Vinuesa, V. van de Pol, M.E. Geerts, M.R. de Vries, S.G.T. Janson, H. van Dam, J.H. Lindeman, M.-J. Goumans, P. ten Dijke, Inflammation induces endothelial-to-mesenchymal transition and promotes vascular calcification through downregulation of BMPR2, J. Pathol. 247 (2019) 333–346, https://doi.org/10.1002/path.5193.

[33] K.M. Drake, B.J. Dunmore, L.N. McNelly, N.W. Morrell, M.A. Aldred, Correction of nonsense BMPR2 and SMAD9 mutations by ataluren in pulmonary arterial hypertension, Am. J. Respir. Cell Mol. Biol. 49 (2013) 403–409, https://doi.org/10.1165/rcmb.2013-0100OC.

[34] Y. Nakamura, K. Tensho, H. Nakaya, M. Nawata, T. Okabe, S. Wakitani, Low dose fibroblast growth factor-2 (FGF-2) enhances bone morphogenetic protein-2 (BMP-2)-induced ectopic bone formation in mice, Bone 36 (2005) 399–407, https://doi.org/10.1016/j.bone.2004.11.010.

[35] H. Lin, Y. Tang, T.P. Lozito, N. Oyster, R.B. Kang, M.R. Fritch, B. Wang, R.S. Tuan, Projection stereolithographic fabrication of BMP-2 gene-activated matrix for bone tissue engineering, Sci. Rep. 7 (2017), 11327, https://doi.org/10.1038/s41598-017-11051-0.

[36] T.A. Einhorn, Enhancement of fracture-healing, J. Bone Joint Surg. Am. 77 (1995) 940–956, https://doi.org/10.2106/00004623-199506000-00016.

[37] D. Gothard, E.L. Smith, J.M. Kanczler, H. Rashidi, O. Qutachi, J. Henstock, M. Rotherham, A. El Haj, K.M. Shakesheff, R.O. Oreffo, Tissue engineered bone using select growth factors: a comprehensive review of animal studies and clinical translation studies in man, Eur. Cell. Mater. 28 (2014) 166–207. ; discussion 207-168, 10.22203/ecm.v028a13.

[38] Z. Chen, Z. Zhang, J. Feng, Y. Guo, Y. Yu, J. Cui, H. Li, L. Shang, Influence of mussel-derived bioactive BMP-2-decorated PLA on MSC behavior in vitro and verification with osteogenicity at ectopic sites in vivo, ACS Appl. Mater. Inter. 10 (2018) 11961–11971, https://doi.org/10.1021/acsami.8b01547.

[39] C.E. Vantucci, L. Krishan, A. Cheng, A. Prather, K. Roy, R.E. Guldberg, BMP-2 delivery strategy modulates local bone regeneration and systemic immune responses to complex extremity trauma, Biomater. Sci. 9 (2021) 1668–1682, https://doi.org/10.1039/D0BM01728K.

[40] Y. Yu, R. Chen, Y. Yuan, J. Wang, C. Liu, Affinity-selected polysaccharide for rhBMP-2-induced osteogenesis via BMP receptor activation, Appl. Mater. Today 20 (2020), 100681, https://doi.org/10.1016/j.apmt.2020.100681.

[41] Z. Huang, D. Sun, J.X. Hu, F.L. Tang, D.H. Lee, Y. Wang, G. Hu, X.J. Zhu, J. Zhou, L. Mei, W.C. Xiong, Neogenin promotes BMP2 activation of YAP and Smad1 and enhances astrocytic differentiation in developing mouse neocortex, J. Neurosci. 36 (2016) 5833, https://doi.org/10.1523/JNEUROSCI.4487-15.2016.

[42] D. Li, K. Yu, T. Xiao, Y. Dai, L. Liu, H. Li, D. Jiang, L. Xiong, LOC103691336/miR-138-5p/BMPR2 axis modulates Mg-mediated osteogenic differentiation in rat femoral fracture model and rat primary bone marrow stromal cells, J. Cell. Physiol. 234 (2019) 21316–21330, https://doi.org/10.1002/jcp.28736.

[43] A.J. Nakamura, Y.J. Chiang, K.S. Hathcock, I. Horikawa, O.A. Sedelnikova, R. J. Hodes, W.M. Bonner, Both telomeric and non-telomeric DNA damage are determinants of mammalian cellular senescence, Epigenet. Chromatin 1 (6) (2008), https://doi.org/10.1186/1756-8935-1-6.

[44] S. Zhang, J. Chen, Y. Yu, K. Dai, J. Wang, C. Liu, Accelerated bone regenerative efficiency by regulating sequential release of BMP-2 and VEGF and synergism with sulfated chitosan, ACS Biomater. Sci. Eng. 5 (2019) 1944–1955, https://doi.org/10.1021/acsbiomaterials.8b01490.

[45] Y. Yu, K. Dai, Z. Gao, W. Tang, T. Shen, Y. Yuan, J. Wang, C. Liu, Sulfated polysaccharide directs therapeutic angiogenesis via endogenous VEGF secretion of macrophages, Sci. Adv. 7 (2021), eabd8217, https://doi.org/10.1126/sciadv.abd8217.

[46] J. Ping, C. Zhou, Y. Dong, X. Wu, X. Huang, B. Sun, B. Zeng, F. Xu, W. Liang, Modulating immune microenvironment during bone repair using biomaterials: focusing on the role of macrophages, Mol. Immunol. 138 (2021) 110–120, https://doi.org/10.1016/j.molimm.2021.08.003.

[47] X. Cao, X. Wu, D. Frassica, B. Yu, L. Pang, L. Xian, M. Wan, W. Lei, M. Armour, E. Tryggestad, J. Wong, C.Y. Wen, W.W. Lu, F.J. Frassica, Irradiation induces bone injury by damaging bone marrow microenvironment for stem cells, Proc. Natl. Acad. Sci. U. S. A. 108 (2011) 1609, https://doi.org/10.1073/pnas.1015350108.

[48] Y. Nakamura, S. Wakitani, J. Nakayama, S. Wakabayashi, H. Horiuchi, K. Takaoka, Temporal and spatial expression profiles of BMP receptors and noggin during BMP-2-induced ectopic bone formation, J. Bone Miner. Res. 18 (2003) 1854–1862, https://doi.org/10.1359/jbmr.2003.18.10.1854.

[49] T.P. Alastalo, M. Li, V. de Jesus Perez, D. Pham, H. Sawada, J.K. Wang, M. Koskenvuo, L. Wang, B.A. Freeman, H.Y. Chang, M. Rabinovitch, Disruption of PPARγ/β-catenin–mediated regulation of apelin impairs BMP-induced mouse and human pulmonary arterial EC survival, J. Clin. Invest. 121 (2011) 3735–3746, https://doi.org/10.1172/JCI43382.

[50] M. Guzman-Ayala, N. Ben-Haim, S. Beck, D.B. Constam, Nodal protein processing and fibroblast growth factor 4 synergize to maintain a trophoblast stem cell microenvironment, Proc. Natl. Acad. Sci. U. S. A. 101 (2004), 15656, https://doi.org/10.1073/pnas.0405429101.

[51] R.M. Tenney, D.E. Discher, Stem cells, microenvironment mechanics, and growth factor activation, Curr. Opin. Cell Biol. 21 (2009) 630–635, https://doi.org/10.1016/j.ceb.2009.06.003.

[52] D. Park, J. Lim, J.Y. Park, S.H. Lee, Concise review: stem cell microenvironment on a chip: current technologies for tissue engineering and stem cell biology, STEM CELLS Transl. Med. 4 (2015) 1352–1368, https://doi.org/10.5966/sctm.2015-0095.

[53] P.B. Yu, D.Y. Deng, C.S. Lai, C.C. Hong, G.D. Cuny, M.L. Bouxsein, D.W. Hong, P. M. McManus, T. Katagiri, C. Sachidanandan, N. Kamiya, T. Fukuda, Y. Mishina, R. T. Peterson, K.D. Bloch, BMP type I receptor inhibition reduces heterotopic ossification, Nat. Med. 14 (2008) 1363–1369, https://doi.org/10.1038/nm.1888.

[54] Y. Pan, J. Chen, Y. Yu, K. Dai, J. Wang, C. Liu, Enhancement of BMP-2-mediated angiogenesis and osteogenesis by 2-N,6-O-sulfated chitosan in bone regeneration, Biomater. Sci. 6 (2018) 431–439, https://doi.org/10.1039/C7BM01006K.

[55] A. Jauković, D. Abadjieva, D. Trivanović, E. Stoyanova, M. Kostadinova, S. Pashova, S. Kestendjieva, T. Kukolj, M. Jeseta, E. Kistanova, M. Mourdjeva, Specificity of 3D MSC spheroids microenvironment: impact on MSC behavior and properties, Stem Cell Rev. Rep. 16 (2020) 853–875, https://doi.org/10.1007/s12015-020-10006-9.

[56] S. Chasan, E. Hesse, P. Atallah, M. Gerstner, S. Diederichs, A. Schenker, K. Grobe, C. Werner, W. Richter, Sulfation of glycosaminoglycan hydrogels instructs cell fate and chondral versus endochondral lineage decision of skeletal stem cells in vivo, Adv. Funct. Mater. n/a (2021), https://doi.org/10.1002/adfm.202109176, 2109176.

[57] A.S. Caldwell, B.A. Aguado, K.S. Anseth, Designing microgels for cell culture and controlled assembly of tissue microenvironments, Adv. Funct. Mater. 30 (2020), 1907670, https://doi.org/10.1002/adfm.201907670.